Journal of Computational Mathematics
Vol.xx, No.x, 2024, 1–19.

http://www.global-sci.org/jcm
doi:10.4208/jcm.2210-m2022-0002

NEAR-FIELD IMAGING OF AN INHOMOGENEOUS CAVITY WITH A MODIFIED FACTORIZATION METHOD*

Yanli Cui and Fenglong Qu[1)]
School of Mathematics and Information Sciences, Yantai University, Yantai 264005, China
Email: cuiyanli@amss.ac.cn, fenglongqu@amss.ac.cn
Xiliang Li
School of Mathematics and Information Science, Shandong Technology and Business University, Yantai 264005, China
Email: lixiliang@amss.ac.cn

Abstract

This paper is concerned with the inverse problem of scattering of time-harmonic acoustic waves by an inhomogeneous cavity. We shall develop a modified factorization method to reconstruct the shape and location of the interior interface of the inhomogeneous cavity by means of many internal measurements of the near-field data. Numerical examples are carried out to illustrate the practicability of the inversion algorithm.

Mathematics subject classification: 35R30, 35Q60, 35P25, 78A46.
Key words: Inverse problems, Acoustic scattering, Numerical reconstruction, Inhomogeneous cavity.

1. Introduction

Consider the inverse scattering problem of recovering the shape and location of the interior interface of an impenetrable inhomogeneous cavity from many internal measurements. This kind of interior scattering problem may occur in many industry and military applications such as in material science, non-destructive testing and so on (cf. [14,32] and the references therein).

In contrast to the typical exterior scattering problem, where the incident field and the associated measurements are taken outside the objects, the interior scattering problem allows the incident point sources and measurements taken inside the cavity. In the current paper we consider the scattering of incident point sources by an inhomogeneous cavity, which is modeled by an inhomogeneous Helmholtz equation with various boundary conditions on the exterior boundary. Our goal is to study the inverse problem of numerically reconstructing the shape and location of the interior interface of the inhomogeneous cavity from the near-field data measured inside the cavity.

There are lots of investigations consisting of theoretical results and numerical methods for the exterior scattering problems in the past decades. We refer to the monographs [6,9,18] and the references quoted therein for detailed discussions. In the mean time the interior scattering problems also attracted many researchers' attention, where the studies are mainly focused on the numerical methods in recovering a homogeneous cavity. For example, the factorization method can be found in [19,21], the linear sampling method has been developed in [7,13,32,33] and a nonlinear integral equation method was established in [23]. It was also noticed that the

* Received January 2, 2022 / Revised version received May 6, 2022 / Accepted October 27, 2022 / Published online February 25, 2024 /
1) Corresponding author

inverse scattering by large cavities embedded in an infinite ground plane has been well studied, see, e.g. [2–4] and the references quoted therein. However, there are few results available in the literature for reconstructing an inhomogeneous cavity. For the case when the refractive index of the inhomogeneous cavity was described by a piecewise constant function, the authors in [24] obtained a uniqueness result on the identification of the interior interface as well as the piecewise constant refractive index, the technique can date back to the work [30], which focused on the shape reconstruction of the exterior inverse scattering problems.

In this paper, we intend to establish a modified factorization method as an analytical and numerical tool of reconstructing the interior interface of the inhomogeneous cavity with different kinds of boundary conditions on the exterior boundary. The factorization method was proposed by the work [15], which can provide a sufficient and necessary computational criterion for characterizing the shape and location of the scatterers. Therefore, it has been widely studied for various inverse scattering problems (cf. [5, 10, 11, 16–18, 25, 29] and the references therein). Recently, based on a technique of the detailed description of the kernel space of the related solution operator, the factorization method has been justified in [26] for the inverse problem of reconstructing the interior interface of a two-layered cavity in the case when the solution is discontinuous across the interior interface, that is, $u|_+ = u|_-$, $\partial_\nu u|_+ = \lambda \partial_\nu u|_-$ on ∂D for $\lambda \neq 1$. Unfortunately, the method developed in [26] is not capable of dealing with the inverse problem under consideration since the solution of our model problem is continuous across the interior interface, which means, $u|_+ = u|_-$, $\partial_\nu u|_+ = \lambda \partial_\nu u|_-$ on ∂D for $\lambda = 1$. This actually yields that the middle operator of the factorization in [26] is only compact for the problem setting we are considering. So, we need to develop a novel numerical algorithm, which is an approximate factorization method constructed depending on both the refractive index in the inhomogeneous medium and the boundary conditions on the exterior boundary, to solve our inverse problem. To be precise, we shall establish a series of perturbation operators N_m of the near field operator N, which is defined on a curve located inside the cavity. It can be proved that for sufficiently large $m_0 \in N_+$, the operator N_{m_0}, which can be viewed as a sufficiently small perturbation of the near field operator N, has a suitable factorization satisfying the Range Identity in [18, Theorem 2.15]. Moreover, $N_{m_0,\#}$ can also be viewed as a sufficient small perturbation of the noisy operator $N^\delta_\#$ with the noise level δ. Then the target interior interface of the inhomogeneous cavity can be approximately determined by means of the spectral data of $N_{m_0,\#}$ and $N^\delta_\#$. Numerical examples provided in Section 4 indeed illustrate the practicability of the proposed approximate factorization method.

The reader is also referred to [5, 15, 27, 28] for the justification of the factorization method for the exterior inverse medium scattering problems, to [1, 12, 31] for the iteration method, and to [8, 22] for the linear sampling method.

The paper is organized as follows. In Section 2, the formulations of the model problem will be presented. Some necessary properties on the solution operator are also provided. Section 3 is devoted to the mathematical establishment of an approximate factorization method for the inverse problem of reconstructing the interior interface of the inhomogeneous cavity. In Section 4, some numerical examples are carried out to illustrate the efficiency of the developed inversion algorithm.

2. Formulations of the Scattering Problem

We begin with the formulations of our scattering problem. Let $D \subset \mathbb{R}^d, d = 2, 3$, be

an inhomogeneous cavity with a C^2 smooth boundary Σ. Assume further that $D = \overline{D_0} \cup D_1$ with $D_0 \cap D_1 = \emptyset$, where D_0, D_1 denote the interior and annular part of the inhomogeneous cavity, respectively. See Fig. 2.1 for the geometry of the scattering problem.

Consider the incident point source located at $y \in D_0$ taking the form

$$u^{\mathrm{i}}(x) := \Phi(x,y) = \begin{cases} \dfrac{i}{4} H_0^{(1)}(k|x-y|) & \text{in } \mathbb{R}^2 \setminus \{y\}, \\ \dfrac{1}{4\pi} \dfrac{e^{ik|x-y|}}{|x-y|} & \text{in } \mathbb{R}^3 \setminus \{y\}, \end{cases} \tag{2.1}$$

where $\Phi(x,y)$ is the fundamental solution of the Helmholtz equation $\triangle\Phi + k^2\Phi = -\delta_y$ in the free space $\mathbb{R}^d$. Then the scattering problem can be formulated in determining the total field u such that

$$\begin{cases} \triangle u + k^2 n(x) u = 0 & \text{in } D \setminus \{y\}, \\ \dfrac{\partial u}{\partial \nu} + \lambda\, u = 0 & \text{on } \Sigma, \\ u = u^{\mathrm{i}} + u^s & \text{in } D, \end{cases} \tag{2.2}$$

where $u^{\mathrm{s}} = u - u^{\mathrm{i}}$ is the scattered wave and $n(x)$ represents the refractive index, which is equal to 1 in D_0. Here $\lambda \neq 1$ is a complex constant, which denotes the transmission coefficient on Σ satisfying that $\mathrm{Im}(\lambda) < 0$ and ν is the unit normal on Σ directed into D_1. Assume further that $0 < \mathrm{Re}(n) < 1$ and $\mathrm{Im}(n) \geq 0$ in D_1. For convenience, we only consider the case when an impedance boundary condition is imposed on the exterior boundary Σ. The same results can be extended in a similar way to other cases such as a Dirichlet boundary condition or a Neumann boundary condition.

Eliminating the incident field u^{i} in D, it is easily seen that the scattered field $v = u^{\mathrm{s}}$ satisfies the following boundary value problem:

$$\begin{cases} \triangle v + k^2 n(x) v = -q f_1 & \text{in } D, \\ \dfrac{\partial v}{\partial \nu} + \lambda\, v = -f_2 & \text{on } \Sigma, \end{cases} \tag{2.3}$$

where

$$q = k^2(n(x) - 1), \quad f_1 = u^{\mathrm{i}}, \quad f_2 = \frac{\partial u^{\mathrm{i}}}{\partial \nu} + \lambda u^{\mathrm{i}}.$$

By applying the variational approach or the integral equation method [24], one can obtain the well-posedness result of the problem (2.3), which is presented in the coming theorem.

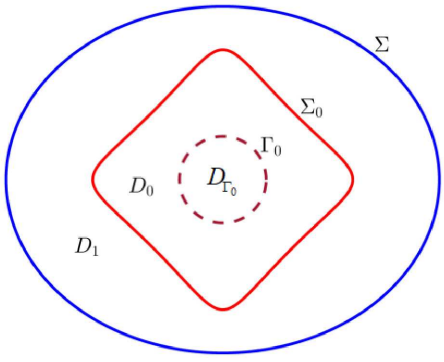

Fig. 2.1. Geometry of the scattering problem.

Theorem 2.1. *For $f_1 \in L^2(D_1)$ and $f_2 \in H^{-1/2}(\Sigma)$ the problem (2.3) admits a unique solution $v \in H^1(D)$ satisfying that*

$$\|v\|_{H^1(D)} \leq C \left(\|f_1\|_{L^2(D_1)} + \|f_2\|_{H^{-\frac{1}{2}}(\Sigma)} \right)$$

with a positive constant $C > 0$.

Based on Theorem 2.1, we define the solution operator $G : X \mapsto L^2(\Gamma_0)$ by

$$G(f_1, f_2)^\top = v|_{\Gamma_0}, \tag{2.4}$$

where v is the solution of the problem (2.3) with the given data

$$(f_1, f_2)^\top \in X := L^2(D_1) \times H^{-\frac{1}{2}}(\Sigma).$$

Here Γ_0 is a closed cure in D_0, which is chosen to be the boundary of a connected open domain D_{Γ_0} satisfying that $\overline{D_{\Gamma_0}} \subset D_0$, and that k^2 is not a Dirichlet eigenvalue of $-\triangle$ in D_{Γ_0}. We then have the properties of the operator G.

Lemma 2.1. *The operator G is compact with dense range in $L^2(\Gamma_0)$.*

Proof. The compactness of the operator G follows from the interior regularity results of the elliptic equations. To prove the denseness of G, it is sufficient to show that its adjoint operator $G^* : L^2(\Gamma_0) \mapsto X^*$ is injective. We first deduce the formulation of G^* and then prove its injectiveness. For $\phi \in L^2(\Gamma_0)$ consider the following boundary value problem:

$$\begin{cases} \triangle w + k^2 w = 0 & \text{in } D_0 \setminus \Gamma_0, \\ \triangle w + k^2 n w = 0 & \text{in } D_1, \\ w|_+ = w|_-, \quad \dfrac{\partial w}{\partial \nu}\Big|_+ - \dfrac{\partial w}{\partial \nu}\Big|_- = \overline{\phi} & \text{on } \Gamma_0, \\ \dfrac{\partial w}{\partial \nu} + \lambda w = 0 & \text{on } \Sigma. \end{cases} \tag{2.5}$$

Here $|_+, |_-$ on Γ_0 indicate the limits to the boundary Γ_0 from inside D_{Γ_0} and $D_0 \setminus \overline{D_{\Gamma_0}}$, respectively, and ν is the unit normal in Γ_0 directed into D_{Γ_0}. Let v be solution of problem (2.3) with the data $(f_1, f_2) \in X$. Then we obtain

$$\left\langle G(f_1, f_2)^\top, \phi \right\rangle_{\Gamma_0} = \int_{\Gamma_0} v \left(\frac{\partial w}{\partial \nu}\Big|_+ - \frac{\partial w}{\partial \nu}\Big|_- \right) ds. \tag{2.6}$$

Applying Green's theorem in D_{Γ_0} and using the boundary conditions on Γ_0 yields

$$\int_{\Gamma_0} \left(v \frac{\partial w}{\partial \nu}\Big|_+ - \frac{\partial v}{\partial \nu} w|_- \right) ds = 0. \tag{2.7}$$

It then follows from (2.6), (2.7), the applications of Green's theorem in $D_0 \setminus \overline{D_{\Gamma_0}}$ and D_1, respectively, and the equations in (2.3) that

$$\begin{aligned} \left\langle G(f_1, f_2)^\top, \phi \right\rangle_{\Gamma_0} &= \int_{\Gamma_0} \left(\frac{\partial v}{\partial \nu} w\Big|_- - v \frac{\partial w}{\partial \nu}\Big|_- \right) ds = \int_{\partial D_0} \left(\frac{\partial v}{\partial \nu} w - v \frac{\partial w}{\partial \nu} \right) ds \\ &= \int_{\Sigma} \left(\frac{\partial v}{\partial \nu} w - v \frac{\partial w}{\partial \nu} \right) ds - \int_{D_1} q f_1 w dx \\ &= -\int_{\Sigma} f_2 w ds - \int_{D_1} q f_1 w dx. \end{aligned} \tag{2.8}$$

So we conclude from (2.8) that

$$G^*\phi = \big(-\overline{qw}|_{D_1}, -\overline{w}|_{\Sigma}\big). \tag{2.9}$$

Now let $G^*\phi = 0$. Thus $w = 0$ in D_1. Hence the Holmgren's uniqueness theorem ensures that $w = 0$ in $D \setminus \overline{D_{\Gamma_0}}$. This means $w|_+ = w|_- = 0$ on Γ_0, which further implies that $w = 0$ in D_{Γ_0}, since k^2 is not a Dirichlet eigenvalue of $-\triangle$ in D_{Γ_0}. Then one has $\phi = 0$ from the transmission conditions on Γ_0. This ends the proof of the lemma. □

3. The Approximate Factorization Method

This section is devoted to the studies on the approximate factorization method in reconstructing the interior interface of the inhomogeneous cavity from many measurements taken on Γ_0. We first introduce the near-field operator $N : L^2(\Gamma_0) \mapsto L^2(\Gamma_0)$ defined by

$$Ng(x) := \int_{\Gamma_0} v(x,z)g(z)ds(z), \quad x \in \Gamma_0, \tag{3.1}$$

where v is the solution of problem (2.3). In order to derive a factorization of the near field operator N, we define the incident operator $H := (H_1, H_2) : L^2(\Gamma_0) \mapsto X$ by

$$H_1 g := \int_{\Gamma_0} \Phi(x,y)g(y)ds(y), \qquad x \in D_1, \tag{3.2}$$

$$H_2 g := \left(\frac{\partial}{\partial\nu(x)} + \lambda\right) \int_{\Gamma_0} \Phi(x,y)g(y)ds(y), \quad x \in \Sigma. \tag{3.3}$$

For $(\phi_1, \phi_2)^\top \in X^*$, it can be derived that

$$\begin{aligned}
\big\langle (H_1, H_2)^\top g, (\phi_1, \phi_2)^\top \big\rangle_{X\times X^*} &= \int_{D_1}\int_{\Gamma_0} \Phi(x,y)g(y)ds(y)\overline{\phi_1}(x)dx \\
&\quad + \int_{\Sigma} \left(\frac{\partial}{\partial\nu(x)} + \lambda\right) \int_{\Gamma_0} \Phi(x,y)g(y)ds(y)\overline{\phi_2}(x)ds(x) \\
&= \int_{\Gamma_0}\int_{D_1} \Phi(x,y)\overline{\phi_1}(x)dxg(y)ds(y) \\
&\quad + \int_{\Gamma_0}\int_{\Sigma} \left(\frac{\partial}{\partial\nu(x)} + \lambda\right) \Phi(x,y)\overline{\phi_2}(x)ds(x)g(y)ds(y) \\
&= \big\langle g, H^*(\phi_1, \phi_2)^\top \big\rangle_{X\times X^*}.
\end{aligned}$$

It follows that $H^*(\phi_1, \phi_2)^\top = w|_{\Gamma_0}$, where the function w is given by

$$w(x) = \int_{D_1} \overline{\Phi(x,y)}\phi_1(y)dy + \int_{\Sigma} \left(\frac{\partial}{\partial\nu(y)} + \lambda\right) \overline{\Phi(x,y)}\phi_2(y)ds(y), \quad x \in D. \tag{3.4}$$

Notice that v is the solution of problem (2.3) corresponding to the incident wave $\Phi(x,y)$. Hence, it is deduced from the definitions of the operator G defined in (2.4), H given in (3.2) and the near-field operator N defined by (3.1) and the superposition principle that $N = GH$. Before going further, we introduce the following operators, which will be frequently used in the rest of the paper. Define

$$(\mathbb{V}\phi)(x) := \int_{D_1} \overline{\Phi(x,y)}\phi(y)dy, \quad x \in D_1,$$

$$(\mathbb{P}\phi)(x) := \int_\Sigma \left(\frac{\partial}{\partial\nu(y)} + \lambda\right) \overline{\Phi(x,y)}\phi(y)ds(y), \quad x \in D_1,$$

and the single- and double-layer operators and their normal derivative operators

$$\begin{aligned}
(S\phi)(x) &:= \int_\Sigma \overline{\Phi(x,y)}\phi(y)ds(y), && x \in \Sigma,\\
(K\phi)(x) &:= \int_\Sigma \frac{\partial\overline{\Phi(x,y)}}{\partial\nu(y)}\phi(y)ds(y), && x \in \Sigma,\\
(K'\phi)(x) &:= \frac{\partial}{\partial\nu(x)}\int_\Sigma \overline{\Phi(x,y)}\phi(y)ds(y), && x \in \Sigma,\\
(T\phi)(x) &:= \frac{\partial}{\partial\nu(x)}\int_\Sigma \frac{\partial\overline{\Phi(x,y)}}{\partial\nu(y)}\phi(y)ds(y), && x \in \Sigma.
\end{aligned}$$

It is known from [6,9] that the operators $S : H^{-1/2}(\Sigma) \mapsto H^{1/2}(\Sigma)$, $K : H^{1/2}(\Sigma) \mapsto H^{1/2}(\Sigma)$, $K' : H^{-1/2}(\Sigma) \mapsto H^{-1/2}(\Sigma)$ and $T : H^{1/2}(\Sigma) \mapsto H^{-1/2}(\Sigma)$ are all bounded and the operators S, K, K' are also compact in the corresponding Sobolev spaces. We also define the restriction operators

$$V\varphi := (\mathbb{V}\phi)|_\Sigma, \quad \tilde{V}\varphi := \frac{\partial}{\nu(x)}(\mathbb{V}\phi)|_\Sigma.$$

By [20] and the boundedness of the trace operator, we deduce that the operators $\mathbb{V} : L^2(D_1) \mapsto H^2(D_1)$, $\mathbb{P} : H^{1/2}(\Sigma) \mapsto H^1(D_1)$, $V : L^2(D_1) \mapsto H^{3/2}(\Sigma)$, $\tilde{V} : L^2(D_1) \mapsto H^{1/2}(\Sigma)$ are all bounded. Therefore, the factorization of the near-field operator N is stated and proved in the following theorem.

Theorem 3.1. *The near-field operator N has the factorization*

$$N = -GA^*G^*,$$

where the matrix operator $A : X^* \mapsto X$ is given by

$$A = -\begin{pmatrix} -q_1 I + \mathbb{V} & \mathbb{P} \\ \tilde{V} + \lambda V & T + \lambda K' + \lambda K + \lambda^2 S \end{pmatrix}.$$

Proof. It is noted that the function defined by (3.4) satisfies the problem (2.3) with the data

$$\begin{aligned}
f_1 &= q_1\phi_1 - \mathbb{V}\phi_1 - \mathbb{P}\phi_2, \quad q_1 = \frac{1}{q},\\
-f_2 &= \tilde{V}\phi_1 + \lambda V\phi_1 + T\phi_2 + \lambda K'\phi_2 + \lambda K\phi_2 + \lambda^2 S\phi_2.
\end{aligned}$$

This can be rewritten as the form of

$$\begin{pmatrix} f_1 \\ f_2 \end{pmatrix} = -\begin{pmatrix} -q_1 I + \mathbb{V} & \mathbb{P} \\ \tilde{V} + \lambda V & T + \lambda K' + \lambda K + \lambda^2 S \end{pmatrix}\begin{pmatrix} \phi_1 \\ \phi_2 \end{pmatrix} = A\phi.$$

By the definition of the operators G and H^*, we have $G(f_1, f_2)^\top = w|_{\Gamma_0} = H^*\phi$, which means $-GA = H^*$. We thus deduce that $H = -A^*G^*$. This together with the fact that $N = GH$ yields the desired result that $N = -GA^*G^*$. This ends the proof of the theorem. □

Theorem 3.2. *The operator A defined in Theorem* 3.1 *is invertible and*

$$A^{-1} = A_1^{-1} + A_{com}, \quad A_1 = \begin{pmatrix} q_1 I & 0 \\ 0 & -T(i) \end{pmatrix},$$

and the operator $T(i)$ is the derivative of the double-layer boundary operator with the wave number $k = i$.

Proof. Obviously, the operator A can be decomposed into the form of

$$A = \begin{pmatrix} q_1 I & 0 \\ 0 & -T(i) \end{pmatrix} - \begin{pmatrix} \mathbb{V} & \mathbb{P} \\ \tilde{V} + \lambda V & T - T(i) + \lambda(K' + K + \lambda S) \end{pmatrix} = A_1 + A_2.$$

It is easily seen that A_1 is invertible on X, since $\mathrm{Re}(n) < 1$ and $-T(i)$ is invertible on $H^{1/2}(\Sigma)$. Clearly, A_2 is compact due to the compactness of the element operators. So one obtains $A = A_1 + A_2$ is a Fredholm type operator. Next we shall show that A is injective. Let $A(\phi_1, \phi_2)^\top = 0$ for some $(\phi_1, \phi_2)^\top \in X^*$. This yields that the function $w(x)$ defined by (3.4) is a solution of the problem (2.3) with the data $(f_1, f_2) = 0$. Thus $w(x) = 0$ in D follows from the uniqueness of (2.3), which combined with the fact that $\triangle w + k^2 w = -\phi_1$ in D_1 immediately leads to that $\phi_1 = 0$. Noting that $w(x)$ defined by (3.4) satisfies the Sommerfeld condition and Helmholtz equation $\triangle w + k^2 w = 0$ in $\mathbb{R}^d \setminus \overline{D}$ with the boundary data $w = 0$ on ∂D. This gives that $w = 0$ in $\mathbb{R}^d \setminus \overline{D}$. Therefore, we derive that $\phi_2 = 0$ by employing the jump relations on Σ. Moreover, by a direct calculation one can easily deduce that $A^{-1} = A_1^{-1} + A_{com}$ with the operator $A_{com} = -A^{-1} A_2 A_1^{-1}$. This completes the proof of the theorem. □

Since $N = GH$ and $H^* = -GA$, we obtain that $N = -H^* A^{-1} H$. In what follows, we attempt to develop a series of perturbation operators N_m of the near-field operator N. Define

$$N_m = N + \rho_m \tilde{H}_2^* T_{\partial\Omega}(i) \tilde{H}_2,$$

where $\rho_m > 0$ satisfying that $\rho_m \longrightarrow 0$ as $m \longrightarrow \infty$, and

$$T_{\partial\Omega}(i) = \frac{\partial}{\partial \nu(x)} \int_{\partial\Omega} \frac{\partial \Phi(x, y, i)}{\partial \nu(y)} \phi(y) ds(y), \quad x \in \partial\Omega.$$

Here $\Phi(x, y, i)$ is the fundamental solution to the Helmholtz equation with the wave number $k = i$ and Ω is chosen satisfying that $D_0 \subsetneq \Omega \subsetneq D$ and the operator $\tilde{H}_2 : L^2(\Gamma_0) \mapsto H^{1/2}(\partial\Omega)$ is defined by

$$\tilde{H}_2 \phi(x) := \int_{\Gamma_0} \Phi(x, y) \phi(y) ds(y), \quad x \in \partial\Omega.$$

It is easy to see that $\tilde{H}_2$ is well defined and bounded. Therefore, we find that

$$\|N_m - N\|_{L^2(\Gamma_0)} = \|\rho_m \tilde{H}_2^* T_{\partial\Omega}(i) \tilde{H}_2\|_{L^2(\Gamma_0)} \cong \rho_m \ \longrightarrow \ 0 \quad \text{as} \quad m \ \longrightarrow \ \infty.$$

We now state some properties for the operator $T_{\partial\Omega}(i)$.

Lemma 3.1. *The operator $-T_{\partial\Omega}(i)$ is self-adjoint and coercive as an operator from $H^{1/2}(\partial\Omega)$ onto $H^{-1/2}(\partial\Omega)$, i.e.*

$$-\int_{\partial\Omega} T_{\partial\Omega}(i) \phi \overline{\phi} ds \geq c \|\phi\|^2_{H^{1/2}(\partial\Omega)}$$

for all $\phi \in H^{1/2}(\partial\Omega)$ with some constant $c > 0$, and the difference $T_{\partial\Omega} - T_{\partial\Omega}(i) : H^{1/2}(\partial\Omega) \to H^{-1/2}(\partial\Omega)$ is compact.

Define the operator $L : H^{1/2}(\partial\Omega) \mapsto H^{-1/2}(\Sigma)$ by

$$Lh := \left(\frac{\partial}{\partial\nu} + \lambda\right) w|_{\Sigma},$$

where w satisfies

$$\begin{cases} \triangle w + k^2 w = 0 & \text{in } \mathbb{R}^d \setminus \overline{\Omega}, \\ w = h & \text{on } \partial\Omega, \\ \dfrac{\partial w}{\partial |x|} - ikw = \mathcal{O}\left(\dfrac{1}{|x|^{d-1}}\right) & \text{as } \ |x| \ \longrightarrow \ \infty \end{cases} \tag{3.5}$$

with $h \in H^{1/2}(\partial\Omega)$. By the well-posedness of the problem (3.5), it can be easily checked that the operator L is well-defined and compact. It is noted that $w := \tilde{H}_2\phi$ is the solution to the problem (3.5), which in combination with the definitions of the operators $L, \tilde{H}_2$ and H_2 yields that $L\tilde{H}_2 = H_2$. Moreover,

$$H = \begin{pmatrix} H_1 \\ H_2 \end{pmatrix} = \begin{pmatrix} I & 0 \\ 0 & L \end{pmatrix} \begin{pmatrix} H_1 \\ \tilde{H}_2 \end{pmatrix} := P\tilde{H}. \tag{3.6}$$

Define the matrix J_m by

$$J_m = \begin{pmatrix} 0 & 0 \\ 0 & \rho_m T_{\partial\Omega}(i) \end{pmatrix}.$$

It thus follows that

$$\rho_m \tilde{H}_2^* T_{\partial\Omega}(i) \tilde{H}_2 = \tilde{H}^* J_m \tilde{H}.$$

This in combination with Theorem 3.1 and (3.6) yields the factorization for the operators N_m that

$$\begin{aligned} N_m &= N + \rho_m \tilde{H}_2^* T_{\partial\Omega}(i) \tilde{H}_2 = H^* A^{-1} H + \tilde{H}^* J_m \tilde{H} = \tilde{H}^* \big[P^* A^{-1} P + J_m\big] \tilde{H} \\ &= \tilde{H}^* \left[P^* \begin{pmatrix} q_1 I & 0 \\ 0 & -T^{-1}(i) \end{pmatrix} P + P^* A_{com} P + J_m \right] \tilde{H} \\ &= \tilde{H}^* \left[\begin{pmatrix} I & 0 \\ 0 & L^* \end{pmatrix} \begin{pmatrix} q_1 I & 0 \\ 0 & -T^{-1}(i) \end{pmatrix} \begin{pmatrix} I & 0 \\ 0 & L \end{pmatrix} + P^* A_{com} P + J_m \right] \tilde{H} \\ &= \tilde{H}^* \begin{pmatrix} q_1 I & 0 \\ 0 & \rho_m T_{\partial\Omega}(i) \end{pmatrix} \tilde{H} + \tilde{H}^* \left[\begin{pmatrix} 0 & 0 \\ 0 & -L^* T^{-1}(i) L \end{pmatrix} + P^* A_{com} P \right] \tilde{H} \\ &= \tilde{H}^* \big(\tilde{M}_m^{(1)} + \tilde{M}_{com}^{(2)}\big) \tilde{H} =: \tilde{H}^* \tilde{M}_m \tilde{H}. \end{aligned} \tag{3.7}$$

In view of the fact that $0 < \mathrm{Re}(n) < 1$ in D_1 and the operator $-T_{\partial\Omega}(i)$ is self-adjoint and coercive as an operator from $H^{1/2}(\partial\Omega)$ onto $H^{-1/2}(\partial\Omega)$, one derives that $-\mathrm{Re}(\tilde{M}_m^{(1)})$ is coercive on $\tilde{X} := L^2(D_1) \times H^{1/2}(\partial\Omega)$. Since the operators L, A_{com} are all compact, which leads to that the operator $\mathrm{Re}(\tilde{M}_{com}^{(2)})$ is compact on $\tilde{X}$. Recalling Lemma 2.1, the fact that $H^* = GA$ and the invertibility of the matrix A implies the coming theorem.

Theorem 3.3. *$\tilde{H}^*$ is compact with dense range in $L^2(S^2)$.*

Proof. With the aid of the fact that $H^* = GA$ and the invertibility of the matrix A, we obtain that $H^* A^{-1} = G$. Recalling $H = P\tilde{H}$ yields $H^* = \tilde{H}^* P^*$. Then we deduce that $\widetilde{H}^* P^* A^{-1} = H^* A^{-1} = G$. Whence the desired result follows from Lemma 2.1. This ends the proof of the theorem. □

Furthermore, we have the following theorem.

Theorem 3.4. *For $z \in \mathbb{R}^d$, it holds that*

$$z \in \mathbb{R}^d \setminus \overline{D_0} \iff \Phi(\cdot, z)|_{\Gamma_0} \in R(\tilde{H}^*),$$

where $\tilde{H}$ is given by (3.6).

Proof. For $z \in \mathbb{R}^d \setminus \overline{D_0}$, we choose a ball $\overline{B_\delta(z)}$ with the center z and the radius $\delta > 0$ satisfying that $\overline{B_\delta(z)} \subset \mathbb{R}^d \setminus \overline{D_0}$. Define a cut-off function $\chi \in C^\infty(\mathbb{R}^d)$ with $\chi(t) = 1$ for $|t| \geq \delta$ and $\chi(t) = 0$ for $|t| \leq \delta/2$. Let

$$v(x) := \chi(|x - z|)\Phi(x, z), \quad x \in \mathbb{R}^d.$$

Clearly, $v(x) \in C^\infty(R^3)$ and $v = \Phi(\cdot, z)$ for $|x - z| \geq \delta$. By direct calculations, it is found that

$$\triangle v + k^2 n v = \Phi \triangle \chi + \chi \triangle \Phi + 2\nabla\chi.\nabla\Phi + k^2 n \chi \Phi = -q f_1 \quad \text{in } D_1,$$

and

$$\left(\frac{\partial v}{\partial \nu} + \lambda v\right)\Big|_\Sigma = f_2.$$

It is obvious that $f_1 \in L^2(D_1)$ and $f_2 \in H^{-1/2}(\Sigma)$. Then v is the solution to the problem (2.3) with the data $(f_1, f_2)^\top \in X$. So we have that $G(f_1, f_2)^\top = v|_{\Gamma_0} = \Phi(\cdot, z)|_{\Gamma_0}$, which means that $\Phi(\cdot, z)|_{\Gamma_0} \in R(G)$. Making use of the fact that $H^* = GA$ and the matrix A is invertible, we obtain that $\Phi(\cdot, z)|_{\Gamma_0} \in H^*$. This together with $H^* = \tilde{H}^* P^*$ yields that $\Phi(\cdot, z)|_{\Gamma_0} \in R(\tilde{H}^*)$.

For $z \notin \mathbb{R}^d \setminus \overline{D_0}$, let $\phi^z = (\phi_1^z, \phi_2^z)^\top \in \tilde{X}^*$ be such that $\tilde{H}^* \phi^z = \Phi_z|_{\Gamma_0}$. Hence, we arrive at that

$$\tilde{H}^* \phi^z = \int_{D_1} \Phi(\cdot, y)\phi_1^z(y)dy + \int_{\partial\Omega} \Phi(\cdot, y)\phi_2^z(y)ds(y) = \Phi(\cdot, z)|_{\Gamma_0} \quad \text{in } D_0 \setminus \{z\}.$$

From the above equality, we find that the left-hand is continuous at z whereas the right-hand is singular at z, which leads to a contradiction. This ends the proof of the theorem. □

To justify the approximate factorization method we need to show the following theorem.

Theorem 3.5. *Let $\tilde{M}_m = \tilde{M}_m^{(1)} + \tilde{M}_{com}^{(2)}$ be defined by* (3.7)*, then*

(i) $\tilde{M}_m^{(1)}$ is coercive and $\tilde{M}_{com}^{(2)}$ is compact.

(ii) $\mathrm{Im}\langle \tilde{M}_m \phi, \phi\rangle > 0$ for all $\phi \in \overline{R(\tilde{H})}$ with $\phi \neq 0$.

Proof. The assertion (i) follows from the properties of $M_m^{(1)}$ and $M_{com}^{(2)}$, see the discussions below (3.7).

(ii) We first show that $\mathrm{Im}\langle \tilde{M}_m \phi, \phi\rangle \geq 0$. Since the operator $T(i)$ is self-adjoint, we find that for $\phi \in \overline{R(\tilde{H})}$,

$$\begin{aligned}
\mathrm{Im}\big\langle \tilde{M}_m \phi, \phi\big\rangle &= \mathrm{Im}\big\langle \big(P^* A^{-1} P + J_m\big)\phi, \phi\big\rangle = \mathrm{Im}\big\langle P^* A^{-1} P\phi, \phi\big\rangle \\
&= \mathrm{Im}\big\langle A^{-1} P\phi, P\phi\big\rangle = \mathrm{Im}\big\langle P\phi, (A^{-1})^* P\phi\big\rangle \\
&= \mathrm{Im}\big\langle A^*\big((A^{-1})^* P\phi\big), (A^{-1})^* P\phi\big\rangle := \langle A^*\psi, \psi\rangle,
\end{aligned}$$

where $\psi := A^{-1*} P\phi$. For $\phi \in \overline{R(\tilde{H})}$, since $H = P\tilde{H}$ one derives that $P\phi \in \overline{R(H)}$. Recalling $H^* = GA$ yields $G^* = A^{-1*} H$, which further implies that $\psi := A^{-1*} P\phi \in R(G^*)$. In order to prove assertion (ii), it suffices to show that

$$\mathrm{Im}\langle \psi, A\psi\rangle \geq 0 \quad \text{for} \quad \psi \in R(G^*).$$

Let $\psi = (\psi_1, \psi_2)$. Define the function

$$\begin{aligned} w(x) &= \int_{D_1} \Phi(x,y)\psi_1(y)dy + \int_\Sigma \left(\frac{\partial}{\partial \nu(y)} + \lambda\right)\Phi(x,y)\psi_2(y)ds(y) \\ &=: w_1 + w_2, \quad x \in \mathbb{R}^d \setminus \Sigma. \end{aligned} \tag{3.8}$$

It is easily seen that w is the solution to the problem (2.3) with the data

$$f_1 = q_1\psi_1 - w, \quad f_2 = -\left(\frac{\partial}{\partial \nu} + \lambda\right) w|_\Sigma.$$

Noting that

$$\psi_2 = w|_+ - w|_-, \quad \lambda\psi_2 = \frac{\partial w}{\partial \nu}\Big|_- - \frac{\partial w}{\partial \nu}\Big|_+, \quad \lambda\psi_2 = \frac{\partial w_2}{\partial \nu}\Big|_- - \frac{\partial w_2}{\partial \nu}\Big|_+ \quad \text{on } \Sigma,$$

where $|_+, |_-$ on Σ indicate the limits to the boundary Σ from inside D and outside $\mathbb{R}^d \setminus \overline{D}$, respectively. One then obtains

$$\begin{aligned} \langle A\psi, \psi\rangle_{X\times X^*} &= \big\langle (f_1, f_2)^\top, (\psi_1, \psi_2)^\top \big\rangle_{X\times X^*} \\ &= \langle q_1\psi_1 - w, \psi_1\rangle_{D_1} - \left\langle \left(\frac{\partial w}{\partial \nu} + \lambda w\right)\Big|_+, \psi_2 \right\rangle_\Sigma \\ &= \langle q_1\psi_1, \psi_1\rangle_{D_1} - \langle w_1, \psi_1\rangle_{D_1} - \langle w_2, \psi_1\rangle_{D_1} - \left\langle \frac{\partial w}{\partial \nu}\Big|_+, \psi_2 \right\rangle_\Sigma \\ &\quad - \lambda\langle w_1|_+, \psi_2\rangle_\Sigma - \lambda\langle w_2|_+, \psi_2\rangle_\Sigma \\ &:= I_1 + I_2 + I_3 + I_4 + I_5 + I_6. \end{aligned}$$

It is obvious that $\mathrm{Im}(I_1) \le 0$ since $\mathrm{Im}(n) \ge 0$. For the term I_2, we have

$$\begin{aligned} I_2 &= -\langle w_1, \psi_1\rangle_{D_1} = \int_{D_1} w_1\big(\triangle\overline{w_1} + k^2\overline{w_1}\big)dx \\ &= \left(\int_{\partial D_0} - \int_\Sigma\right) w_1 \frac{\partial \overline{w_1}}{\partial \nu} ds - \int_{D_1} |\nabla w_1|^2 dx + \int_{D_1} k^2 |w_1|^2 dx. \end{aligned}$$

Making use of the Green's theorem in D_0 and $B_R \setminus \overline{D_0}$, respectively, we deduce that

$$\mathrm{Im}(I_2) = -\left\langle w_1, \frac{\partial w_1}{\partial \nu}\right\rangle_\Sigma.$$

For the term I_3, it is found that

$$\begin{aligned} I_3 &= -\langle w_2, \psi_1\rangle_{D_1} = \int_{D_1} w_2\big(\triangle\overline{w}_1 + k^2\overline{w}_1\big)dx \\ &= \int_{\partial D_0} w_2 \frac{\partial \overline{w_1}}{\partial \nu} ds - \left\langle w_2|_+, \frac{\partial w_1}{\partial \nu}\Big|_+\right\rangle_\Sigma - \int_{D_1} \big(\nabla w_2 \cdot \nabla\overline{w}_1 - k^2 w_2\overline{w}_1\big)dx. \end{aligned}$$

For the term I_4, we have

$$-I_4 = \left\langle \frac{\partial w}{\partial \nu}\Big|_+, \psi_2\right\rangle_\Sigma = \left\langle \frac{\partial w}{\partial \nu}\Big|_-, \psi_2\right\rangle_\Sigma - \lambda\langle \psi_2, \psi_2\rangle_\Sigma.$$

We next deal with the term $\langle(\partial w/\partial\nu)|_-, \psi_2\rangle_\Sigma$:

$$\left\langle \frac{\partial w}{\partial \nu}\Big|_-, \psi_2 \right\rangle_\Sigma = \left\langle \frac{\partial w}{\partial \nu}\Big|_-, w|_+ - w|_- \right\rangle_\Sigma = \left\langle \frac{\partial w}{\partial \nu}\Big|_-, w|_+ \right\rangle_\Sigma - \left\langle \frac{\partial w}{\partial \nu}\Big|_-, w|_- \right\rangle_\Sigma,$$

$$\begin{aligned}\left\langle \frac{\partial w}{\partial \nu}\Big|_-, w|_+ \right\rangle_\Sigma &= \left\langle \frac{\partial w_1}{\partial \nu}\Big|_-, w_1|_+ \right\rangle_\Sigma + \left\langle \frac{\partial w_1}{\partial \nu}\Big|_-, w_2|_+ \right\rangle_\Sigma \\ &\quad + \left\langle \frac{\partial w_2}{\partial \nu}\Big|_-, w_1|_+ \right\rangle_\Sigma + \left\langle \frac{\partial w_2}{\partial \nu}\Big|_-, w_2|_+ \right\rangle_\Sigma,\end{aligned}$$

$$\left\langle \frac{\partial w}{\partial \nu}\Big|_-, w|_- \right\rangle_\Sigma = \int_\Sigma \frac{\partial w}{\partial \nu}\Big|_- \overline{w}|_- ds = \int_{\partial B_R} \frac{\partial w}{\partial \nu}\overline{w} ds + \int_{B_R\setminus\overline{D}} \big(|\nabla w|^2 - k^2|w|^2\big) dx.$$

It then follows that

$$\begin{aligned}-\mathrm{Im}(I_4) = \mathrm{Im}\bigg(&\int_{\partial B_R} \frac{\partial w}{\partial \nu}\overline{w} ds + \left\langle \frac{\partial w_1}{\partial \nu}\Big|_-, w_1|_- \right\rangle_\Sigma + \left\langle \frac{\partial w_1}{\partial \nu}\Big|_-, w_2|_+ \right\rangle_\Sigma \\ &+ \left\langle \frac{\partial w_2}{\partial \nu}\Big|_-, w_1|_+ \right\rangle_\Sigma + \left\langle \frac{\partial w_2}{\partial \nu}\Big|_-, w_2|_+ \right\rangle_\Sigma \bigg).\end{aligned}$$

By using the jump relations on Σ, we obtain that

$$-I_5 = \lambda\langle w_1|_+, \psi_2\rangle_\Sigma = \left\langle w_1|_+, \frac{\partial w_2}{\partial \nu}\Big|_- \right\rangle_\Sigma - \left\langle w_1|_+, \frac{\partial w_2}{\partial \nu}\Big|_+ \right\rangle_\Sigma.$$

For the term $\langle w_1|_+, (\partial w_2/\partial\nu)|_+\rangle_\Sigma$, applying the Green's theorem in D_1 yields

$$\left\langle w_1|_+, \frac{\partial w_2}{\partial \nu}\Big|_+ \right\rangle_\Sigma = \int_{\partial D_0} w_1 \frac{\partial \overline{w_2}}{\partial \nu} ds - \int_{D_1} \big(\nabla w_1 \cdot \nabla \overline{w}_2 - k^2 w_1 \overline{w}_2\big) dx.$$

This in combination with the term I_3 and the applications of the Green's theorem in D_0 imply that

$$-\mathrm{Im}(I_3 + I_5) = \mathrm{Im}\left\langle w_1|_+, \frac{\partial w_2}{\partial \nu}\Big|_- \right\rangle_\Sigma + \mathrm{Im}\left\langle w_2|_+, \frac{\partial w_1}{\partial \nu}\Big|_+ \right\rangle_\Sigma.$$

It is further found that

$$-I_6 = \lambda\langle w_2, \psi_2\rangle_\Sigma = \left\langle w_2|_+, \frac{\partial w_2}{\partial \nu}\Big|_- \right\rangle - \left\langle w_2|_+, \frac{\partial w_2}{\partial \nu}\Big|_+ \right\rangle.$$

Therefore, making use of the fact that

$$\begin{aligned}&\mathrm{Im}\left\langle w_1|_+, \frac{\partial w_2}{\partial \nu}\Big|_- \right\rangle_\Sigma + \mathrm{Im}\left\langle \frac{\partial w_2}{\partial \nu}|_-, w_1\Big|_+ \right\rangle_\Sigma = 0, \\ &\mathrm{Im}\left\langle w_2|_+, \frac{\partial w_1}{\partial \nu}\Big|_- \right\rangle_\Sigma + \mathrm{Im}\left\langle \frac{\partial w_1}{\partial \nu}|_-, w_2\Big|_+ \right\rangle_\Sigma = 0, \\ &\mathrm{Im}\left\langle \frac{\partial w_2}{\partial \nu}|_-, w_2\Big|_+, \right\rangle_\Sigma + \mathrm{Im}\left\langle w_2|_+, \frac{\partial w_2}{\partial \nu}\Big|_- \right\rangle_\Sigma = 0,\end{aligned}$$

we conclude from the above analysis for the terms $I_1 - I_6$, the fact that $\mathrm{Im}(\lambda) < 0$ and the Sommerfeld radiation condition that

$$\begin{aligned}\mathrm{Im}\langle A\psi, \psi\rangle_{X\times X^*} &= \int_{\partial B_R} \frac{\partial w}{\partial \nu}\overline{w} ds + \mathrm{Im}(\lambda)\langle \psi_2, \psi_2\rangle_\Sigma \\ &= -\frac{k}{(4\pi)^2}\int_{S^2} |w^\infty|^2 ds + \mathrm{Im}(\lambda)\langle \psi_2, \psi_2\rangle_\Sigma \le 0, \quad \forall\, \psi \in \overline{R(G^*)}, \quad \psi \neq 0,\end{aligned}$$

where w^∞ is the far-field pattern of w defined by (3.8).

Let $\mathrm{Im}\langle A\psi,\psi\rangle_{X\times X^*}=0$ for some $\psi\in\overline{R(G^*)}$. Thus, one immediately obtains that $w^\infty=0$ and $\psi_2=0$. So, $w=0$ in $\mathbb{R}^d\setminus\overline{D}$ follows from Rellich's Lemma. Since $-\overline{\psi}\in\overline{R(G^*)}$, there exists a sequence $\{g_j\}\subset L^2(\Gamma_0)$ satisfying that $G^*g_j\to-\overline{\psi}$ as $j\to\infty$.

It is known from (2.9) that

$$(qp_j|_{D_1},p_j|_\Sigma)\ \to\ \psi\quad\text{as}\quad j\ \to\ \infty, \tag{3.9}$$

where p_j is the solution of the problem (2.5) associated with the boundary data $\phi=g_j$ on Γ_0. Define w_j to be w as in (3.8) with $\psi_1:=qp_j|_{D_1}$ and $\psi_2:=p_j|_\Sigma$. It then follows from (3.9) that $\|w_j-w\|_{H^1(D_1)}\to0$ as $j\to\infty$. Since

$$w_j(x)=\int_{D_1}\Phi(x,y)q(y)p_j(y)dy+\int_\Sigma\left(\frac{\partial}{\partial\nu(y)}+\lambda\right)\Phi(x,y)p_jds(y),\quad x\in\mathbb{R}^d\setminus\Sigma, \tag{3.10}$$

it is easily seen that $\triangle w_j+k^2w_j=-qp_j$ in D_1. Moreover, applying Green's representation theorem leads to that

$$\begin{aligned}p_j(x)=&\int_{\partial D_0}\left\{\frac{\partial p_j(y)}{\partial\nu(y)}\Phi(x,y)-p_j(y)\frac{\partial\Phi(x,y)}{\partial\nu(y)}\right\}ds(y)\\&+\int_{D_1}\Phi(x,y)q(y)p_j(y)dy+\int_\Sigma\left(\frac{\partial}{\partial\nu(y)}+\lambda\right)\Phi(x,y)p_j(y)ds(y),\quad x\in D_1.\end{aligned}$$

This in combination with (3.10) and the transmission conditions on Γ_0 in the problem (2.5) implies that

$$\begin{aligned}p_j(x)-w_j(x)&=\int_{\partial D_0}\left\{\frac{\partial p_j(y)}{\partial\nu(y)}\Phi(x,y)-p_j(y)\frac{\partial\Phi(x,y)}{\partial\nu(y)}\right\}ds(y)\\&=\int_{\Gamma_0}\left\{\frac{\partial p_j(y)}{\partial\nu(y)}|_+\Phi(x,y)-p_j(y)|_+\frac{\partial\Phi(x,y)}{\partial\nu(y)}\right\}ds(y)\\&=\int_{\Gamma_0}\left\{\left(\frac{\partial p_j(y)}{\partial\nu(y)}|_--\overline{g_j(y)}\right)\Phi(x,y)-p_j(y)|_+\frac{\partial\Phi(x,y)}{\partial\nu(y)}\right\}ds(y)\\&=-\int_{\Gamma_0}\Phi(x,y)\overline{g_j(y)}ds(y)=:v_j(x),\quad x\in D_1.\end{aligned} \tag{3.11}$$

From (3.11) it is seen that p_j-w_j can be extended into $\mathbb{R}^d\setminus\overline{D}$ by v_j and

$$v_j\ \to\ \frac{\psi_1}{q}-w\quad\text{in}\ L^2(D_1), \tag{3.12}$$

as $j\to\infty$. Since $\psi_2=0$ and $w=0$ in $\mathbb{R}^d\setminus\overline{D}$ and $\partial p_j/\partial\nu+\lambda p_j=0$ on Σ, we conclude that $v_j\to v$, as $j\to\infty$, where v satisfies the following boundary value problem:

$$\begin{cases}\triangle v+k^2v=0 & \text{in}\ \mathbb{R}^d\setminus\overline{D},\\ \dfrac{\partial v}{\partial\nu}+\lambda v=0 & \text{on}\ \Sigma,\\ \dfrac{\partial v}{\partial|x|}-ikv=\mathcal{O}\left(\dfrac{1}{|x|^{d-1}}\right) & \text{as}\quad |x|\ \longrightarrow\ \infty.\end{cases} \tag{3.13}$$

The uniqueness of the problem (3.13) gives $v=0$ in $\mathbb{R}^d\setminus\overline{D}$, which together with the unique continuation principle yields that $v=0$ in D_1. On the other hand, it is deduced from (3.8) and

(3.13) that w satisfies the equation that $\triangle w + k^2 w = -qv = 0$ in D_1. So that, w is a solution of the Helmholtz equation $\triangle w + k^2 w = 0$ in D with the boundary data $\partial w/\partial \nu = w = 0$ on ∂D. Hence we conclude that $w = 0$ in D, which further means that $\psi_1 = 0$ since $\triangle w + k^2 w = -\psi_1$ in D_1. This completes the proof of the theorem. □

Relying on Theorems 3.4 and 3.5, we are now in a position to provide a sufficient and necessary computational criterion for reconstructing the interior part D_0 of the inhomogeneous cavity.

Theorem 3.6. *For $z \in \mathbb{R}^d$, let $\phi_z := \Phi(\cdot, z)|_{\Gamma_0}$ with $\Phi(\cdot, z)$ be given by (2.1). Then*

$$z \in \mathbb{R}^d \setminus \overline{D_0} \iff W(z) := \left[\sum_j \frac{|\langle \phi_z, \psi_j \rangle_{L^2(\Gamma_0)}|^2}{\lambda_j} \right]^{-1} > 0, \tag{3.14}$$

where $\{\lambda_j; \psi_j\}_{j \in \mathbb{N}}$ is an eigen-system of the self-adjoint operator $N_\# := |\mathrm{Re}(N)| + |\mathrm{Im}(N)|$.

Proof. The proof follows from the range identity [18, Theorem 2.15] in conjunction with Theorems 3.4 and 3.5 and Picard's range criterion. □

Remark 3.1. Theorem 3.6 can be similarly extended to the Dirichlet boundary value problem, that is, $u = 0$ on the exterior boundary Σ or the Neumann boundary value problem, i.e. $\partial u/\partial \nu = 0$ on the exterior boundary Σ. It is remarked that the similar results as that of Theorem 3.6 can also be derived for the case when $\mathrm{Re}(n) > 1$ with different kinds of boundary conditions. The numerical experiments carried out in Section 4 also show that the inversion algorithms are valid.

4. The Numerical Implementation of the Reconstruction of D_0

In this section, the practicability of our developed reconstruction method is studied by carrying out several numerical experiments in $\mathbb{R}^2$. In all numerical examples, the measurement curve Γ_0 is chosen to be a circle. The scattered field data $u^s(x, y)$ is discretized for a finite number of measurement points $x_i \in \Gamma_0$ and source points $y_j \in \Gamma_0$ for $i, j = 1, 2, \ldots, M$, which are equidistantly distributed on the chosen curve Γ_0. In what follows, we shall use the integral equation method with the Nyström algorithm (see, e.g. [9]) to generate the synthetic scattered field data. Hence, the measured data can be derived as the matrix $N_M = (u^s(x_i, y_j)) \in \mathbb{C}^{M \times M}$. So that the indicator function $W(z)$ defined by (3.14) could be approximated as follows:

$$W_M(z) = \left[\sum_{p=1}^{M} \frac{1}{\lambda_p} \left| \sum_{q=1}^{M} \phi_{z,q} \overline{\psi_{p,q}} \right|^2 \right]^{-1} \quad \text{for} \quad z \in \mathbb{R}^2. \tag{4.1}$$

Here $\{\lambda_p; \psi_p\}_{p=1}^M$ is the eigen-system of the self-adjoint matrix

$$N_{M,\#} := |\mathrm{Re}(N_M)| + |\mathrm{Im}(N_M)|$$

with $\psi_p = (\psi_{p,q})_{q=1}^M$ and $\{\phi_{z,q}\}_{q=1}^M$ is the discretization of the test function ϕ_z. Based on Theorem 3.6, it is expected that $W_M(z)$ is much smaller for $z \in D_0$ compared with that for $z \notin D_0$.

In all numerical examples, we shall also show the viability of the developed numerical method from the view of noisy data. The noisy data u_δ^s is simulated by

$$u_\delta^s(x_i, y_j) = u^s(x_i, y_j) + \delta(\xi_1 + i\xi_2)|u^s(x_i, y_j)|$$

for $i, j = 1, 2, \ldots, M$, where $\delta > 0$ is called the noise ratio and ξ_1, ξ_2 are random numbers normally distributed in $[-1, 1]$. Therefore, the perturbed matrix with noisy level δ is given by

$$N_M^\delta := \big(u_\delta^s(x_i, y_j)\big) \in \mathbb{C}^{M\times M},$$
$$(N_M^\delta)_\# := \big|\mathrm{Re}\big(N_M^\delta\big)\big| + \big|\mathrm{Im}\big(N_M^\delta\big)\big|.$$

By using the similar arguments as that in the formula (4.1), the truncated indicator function $W_M^\delta(z)$ can be computed from the eigen-system of the perturbed matrix $(N_M^\delta)_\#$.

In the following examples, we set $M = 64$ or $M = 128$ and use the test curves given in Table 4.1. And $W_M(z)$ is for (b) and $W_M(z)^\delta$ for (c), (d) in Figs. 4.1, 4.3, 4.4, 4.6.

Table 4.1: Parametrization of the curve.

Curve type	**Parametrization**
Circle shaped	$x(t) = R(\cos t, \sin t)$, $t \in [0, 2\pi]$, $R > 0$
Ellipse shaped	$x(t) = (5\cos t, 4\sin t)$, $t \in [0, 2\pi]$
Rounded square (large)	$x(t) = (3/2)(\cos^3 t + \cos t, \sin^3 t + \sin t)$, $t \in [0, 2\pi]$
Rounded square (small)	$x(t) = (3/4)(\cos^3 t + \cos t, \sin^3 t + \sin t)$, $t \in [0, 2\pi]$
Peanut shaped	$x(t) = \sqrt{\cos^2 t + 0.25\sin^2 t}(\cos t, \sin t)$, $t \in [0, 2\pi]$

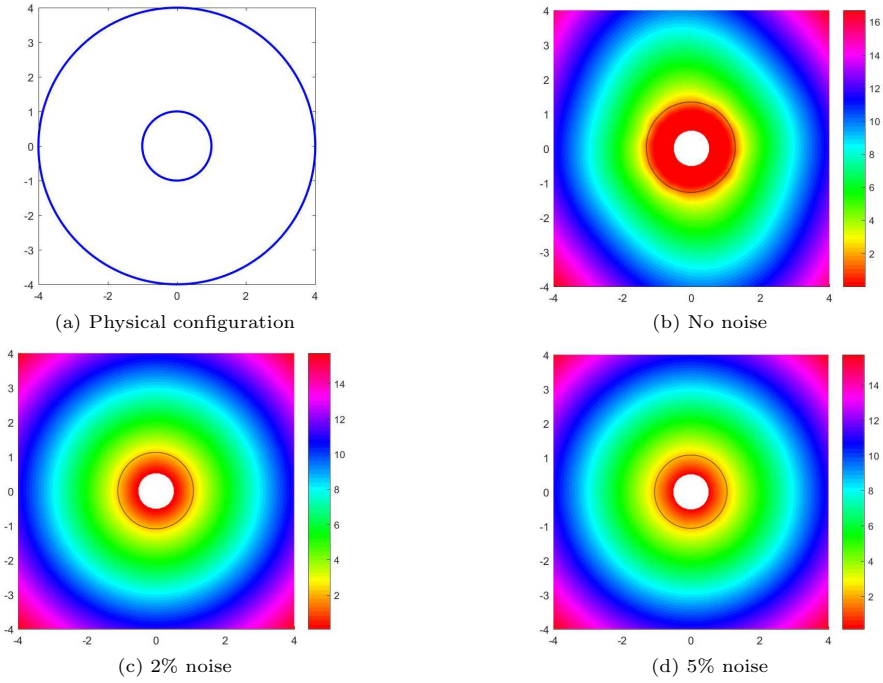

(a) Physical configuration (b) No noise

(c) 2% noise (d) 5% noise

Fig. 4.1. Reconstruction of circle-shaped interface Σ_0. The circle-shaped boundary Σ is sound soft. The wavenumbers are $k1 = 2, k = 1$ and $M = 64$.

Example 4.1. In this example, we consider the case when the Dirichlet boundary condition is imposed on the exterior boundary Σ, that is, Σ is a sound-soft, circle-shaped boundary with radius $R = 4$ and center at $(0, 0)$, and the interior interface Σ_0 is circle-shaped with radius $R = 1$ and center at $(0, 0)$. See Fig. 4.3(a) for the physical configuration. Here the wave numbers are $k1 = 2$ and $k = 1$. For the inverse problem, the measurement curve Γ_0 is chosen to be the circle with radius $R = 0.5$ and center at $(0, 0)$. The reconstruction results of the interface Σ_0 are presented in Fig. 4.3 by using the scattered-field data without noise, with 2% noise and with 5% noise, respectively. In Fig. 4.2, we also provide the comparison of the imaging function $W_M(z)$ defined by (4.1) at $x = 0.4, 0.8, 3.2$ for Fig. 4.1(b).

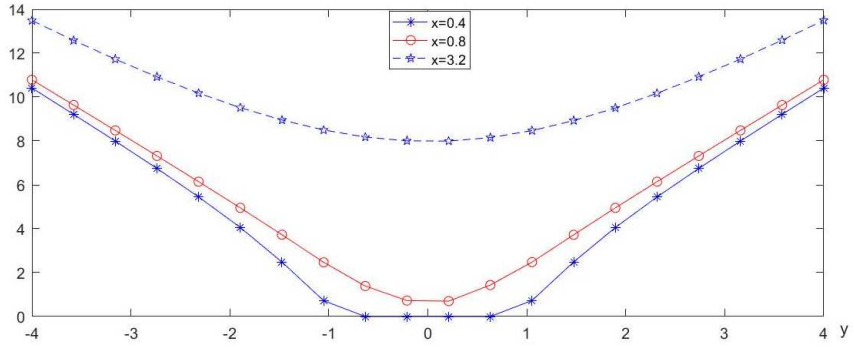

Fig. 4.2. Comparison of the imaging function $W_M(z)$ defined by (4.1) at $x = 0.4, 0.8, 3.2$ for Fig. 4.1(b).

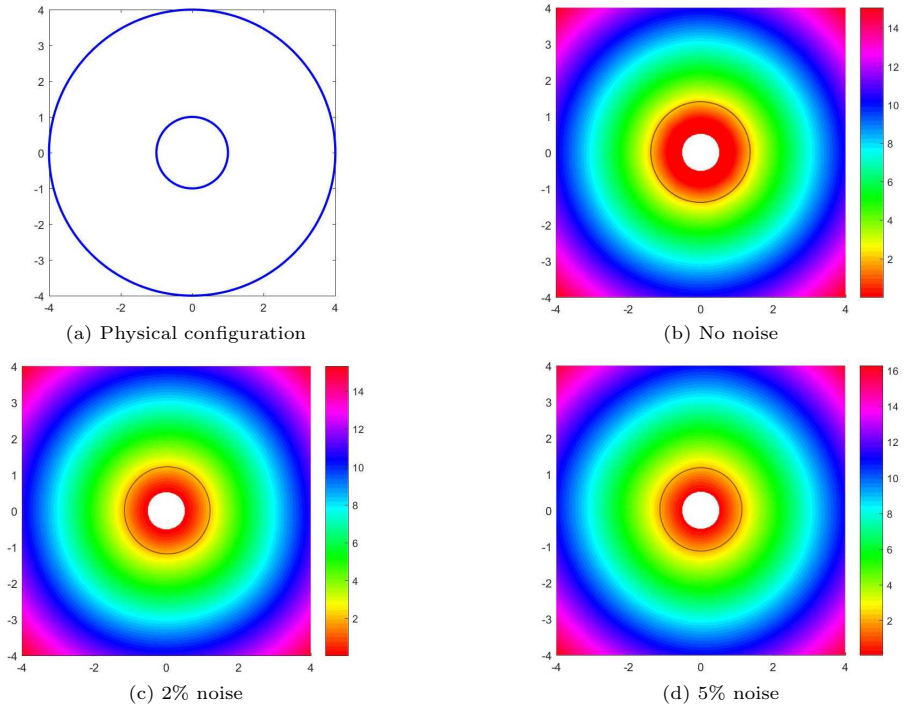

(a) Physical configuration (b) No noise

(c) 2% noise (d) 5% noise

Fig. 4.3. Reconstruction of circle-shaped interface Σ_0. The circle-shaped boundary Σ is sound soft. The wavenumbers are $k1 = 2, k = 1$ and $M = 128$.

Example 4.2. In this example, we consider the case when the Neumann boundary condition is imposed on the exterior boundary Σ, that is, Σ is a sound-hard, rounded square-shaped boundary, and the interior interface Σ_0 is peanut-shaped. See Fig. 4.4(a) for the physical configuration. Moreover, the wave numbers are $k1 = 1+2i$ and $k = 2$. For the inverse problem, the measurement curve Γ_0 is chosen to be the circle with radius $R = 0.3$ and center at $(0, 0)$. The reconstruction results of the interface Σ_0 are presented in Fig. 4.4 by using the scattered-field data without noise, with 2% noise and with 5% noise, respectively. In Fig. 4.5, we also provide the comparison of the imaging function $W_M(z)$ defined by (4.1) at $x = 0.4, 0.8, 3.2$ for Fig. 4.4(b).

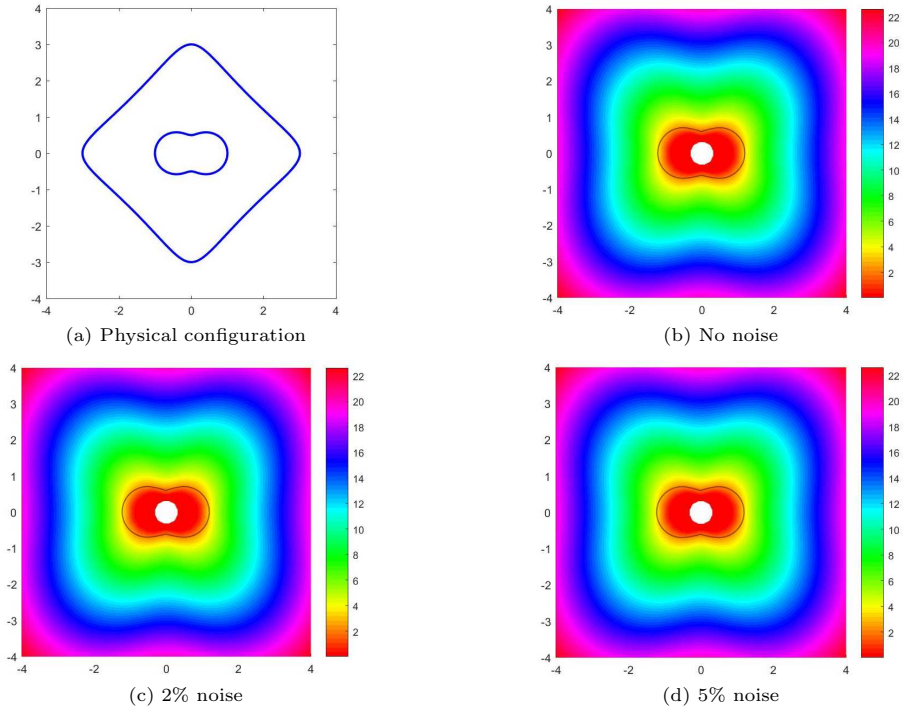

(a) Physical configuration (b) No noise

(c) 2% noise (d) 5% noise

Fig. 4.4. Reconstruction of peanut-shaped interface Σ_0. The rounded square-shaped boundary Σ is sound hard. The wavenumbers are $k1 = 1 + 2i, k = 2$ and $M = 64$.

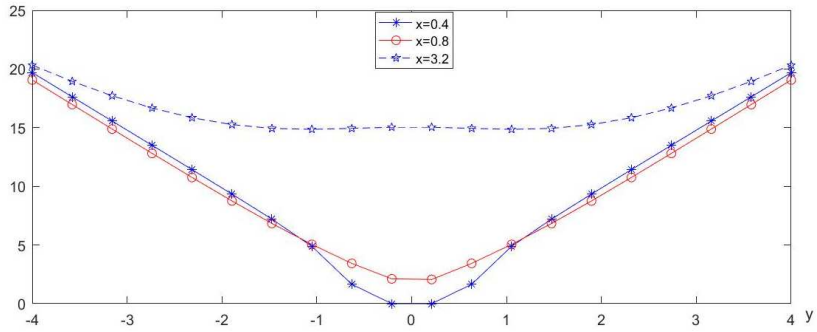

Fig. 4.5. Comparison of the imaging function $W_M(z)$ defined by (4.1) at $x = 0.4, 0.8, 3.2$ for Fig. 4.4(b).

Example 4.3. In this example, we consider the case when the impedance boundary condition is imposed on the exterior boundary Σ, that is, Σ is ellipse-shaped boundary, and the interior interface Σ_0 is rounded square-shaped. See Fig. 4.6(a) for the physical configuration. Moreover, the wave numbers are $k1 = 0.8 + 5i$ and $k = 1$ and the impedance coefficient is given by $\beta(x(t)) = 2+\cos(t), t \in [0, 2\pi]$. For the inverse problem, the measurement curve Γ_0 is chosen to be the circle with radius $R = 0.7$ and center at $(0, 0)$. The reconstruction results of the interface Σ_0 are presented in Fig. 4.6 by using the scattered-field data without noise, with 2% noise and with 5% noise, respectively. In Fig. 4.7, we also provide the comparison of the imaging function $W_M(z)$ defined by (4.1) at $x = 0.4, 0.8, 3.2$ for Fig. 4.6(b).

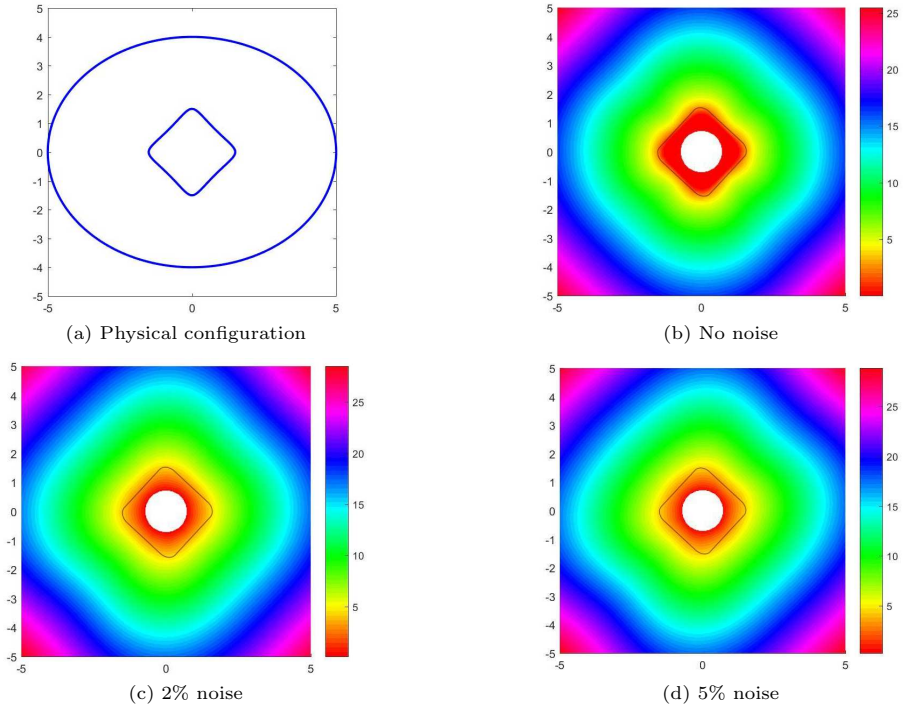

(a) Physical configuration (b) No noise

(c) 2% noise (d) 5% noise

Fig. 4.6. Reconstruction of rounded square-shaped interface Σ_0. The ellipse-shaped boundary Σ is imposed with impedance boundary condition. The wavenumbers are $k1 = 0.8 + 5i, k = 1, M = 64$ and the impedance coefficient is given by $\beta(x(t)) = 2 + \cos(t), t \in [0, 2\pi]$.

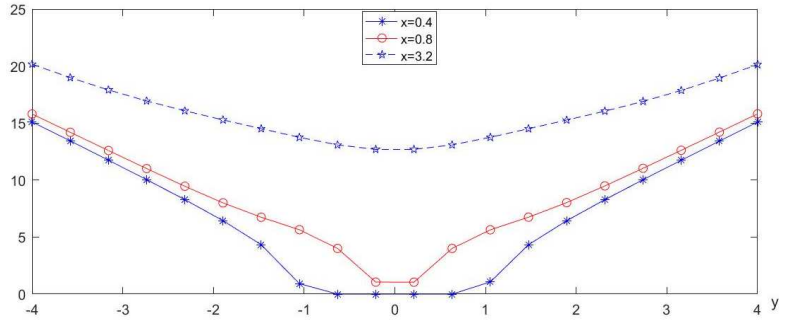

Fig. 4.7. Comparison of the imaging function $W_M(z)$ defined by (4.1) at $x = 0.4, 0.8, 3.2$ for Fig. 4.6(b).

5. Conclusion

We have presented the numerical results of some preliminary examples for approximately reconstructing the interior part of the inhomogeneous cavity with different kinds of boundary conditions imposed on the exterior boundary Σ. From the above four numerical examples and the other cases carried out but not presented here it is shown that the inversion algorithm based on the developed approximate factorization method obtains satisfactory reconstructions of the interior part D_0. It is also seen from the numerical Example 4.1 for different truncation numbers $M = 64$ and $M = 128$ (see Figs. 4.1 and 4.3) that the reconstructed result does not seem obviously better for case when $M = 128$ than that for the case when $M = 64$. This allows us to choose the truncation number $M = 64$ in the following numerical experiments, which also needs less time to be carried out. In fact, the truncation number M is related to the computational result of the scattered wave field u^s. Usually, if the truncation number M is larger, the corresponding computational result is more better. So we conclude that if the reconstruction result is satisfactory for some fixed M, we can not obtain more better results even for the larger M. Moreover, it is found from the mathematical analysis and the numerical experiments that the physical property (i.e. the boundary conditions) of the exterior boundary Σ is not needed to be known in advance. In the future, we plan to extend the method to the cases of inverse elastic scattering or inverse electromagnetic scattering which are more challenging.

Acknowledgements. The work of Y. Cui and F. Qu was supported by the National Natural Science Foundation of China (Grant Nos. 11871416, 12171057) and by the Natural Science Foundation of Shandong Province (Grant No. ZR2019MA027). The work of Xiliang Li is partially supported by the National Natural Science Foundation of China (Grant Nos. 11971273, 12126426) and by the Natural Science Foundation of Shandong Province (Grant No. ZR2018MA004).

References

[1] A. Altundag and R. Kress, On a two-dimensional inverse scattering problem for a dielectric, *Appl. Anal.*, **91** (2012), 757–771.

[2] G. Bao and J. Lai, Optimal shape design of a cavity for radar cross section reduction, *SIAM J. Control Opt.*, **52** (2014), 2122–2140.

[3] G. Bao and P. Li, Inverse medium scattering problems for electromagnetic waves, *SIAM J. Appl. Math.*, **65** (2005), 2049–2066.

[4] G. Bao and W. Sun, A fast algorithm for the electromagnetic scattering from a large cavity, *SIAM J. Sci. Comput.*, **27** (2005), 553–574.

[5] O. Bondarenko, A. Kirsch, and X. Liu, The factorization method for inverse acoustic scattering in a layered medium, *Inverse Problems*, **29**, (2013), 045010.

[6] F. Cakoni and D. Colton, *Qualitative Method in Inverse Scattering Theory*, Springer, 2006.

[7] F. Cakoni, D. Colton, and S. Meng, The inverse scattering problem for a penetrable cavity with internal measurements, *AMS Contemp. Math.*, **615** (2014), 71–88.

[8] F. Cakoni, M. Di Cristo, and J. Sun, A multistep reciprocity gap functional method for the inverse problem in a multi-layered medium, *Complex Variables Elliptic Equ.*, **57**, (2012), 261–276.

[9] D. Colton and R. Kress, *Inverse Acoustic and Electromagnetic Scattering Theory*, Springer, 2013.

[10] D. Colton, R. Kress, and P. Monk, Inverse scattering from an orthotropic medium, *J. Comput. Appl. Math.*, **81** (2007), 269–298.

[11] M. Di Cristo and J. Sun, The determination of the support and surface conductivity of a partially coated object, *Inverse Problems*, **23** (2007), 1161–1179.
[12] T. Hohage and C. Schormann, A Newton-type method for a transmission problem in inverse scattering, *Inverse Problems*, **14** (1998), 1207–1227.
[13] Y. Hu, F. Cakoni, and J. Liu, The inverse scattering problem for a partially coated cavity with interior measurements, *Appl. Anal.*, **93**, (2014), 936–956.
[14] P. Jakubik and R. Potthast, Testing the integrity of some cavity – the Cauchy problem and the range test, *Appl. Numer. Math.*, **58** (2008), 899–914.
[15] A. Kirsch, Characterization of the shape of a scattering obstacle using the spectral data of the far field operator, *Inverse Problems*, **14** (1998), 1489–1512.
[16] A. Kirsch, Factorization of the far field operator for the inhomogeneous medium case and an application in inverse scattering theory, *Inverse Problems*, **15** (1999), 413–429.
[17] A. Kirsch, The MUSIC-algorithm and the factorization method in inverse scattering theory for inhomogeneous media, *Inverse Problems*, **18** (2002), 1025–1040.
[18] A. Kirsch and N. Grinberg, *The Factorization Method for Inverse Problems*, Oxford University Press, 2008.
[19] X. Liu, The factorization method for cavities, *Inverse Problems*, **30** (2014), 015006.
[20] W. McLean, *Strongly Elliptic Systems and Boundary Integral Equations*, Cambridge University Press, 2000.
[21] S. Meng, H. Haddar, and F. Cakoni, The factorization method for a cavity in an inhomogeneous medium, *Inverse Problems*, **30** (2014), 045008.
[22] W. Muniz, A modified linear sampling method valid for all frequencies and an application to the inverse inhomogeneous medium problem, *Proc. Appl. Math. Mech.*, **5** (2005), 689–690.
[23] H. Qin and F. Cakoni, Nonlinear integral equations for shape reconstruction in the inverse interior scattering problem, *Inverse Problems*, **27** (2011), 035005.
[24] F. Qu and J. Yang, On recovery of an inhomogeneous cavity in inverse acoustic scattering, *Inverse Probl. Imaging*, **12** (2018), 281–291.
[25] F. Qu, J. Yang, and B. Zhang, An approximate factorization for inverse medium scattering with unknown buried objects, *Inverse Problems*, **33** (2017), 035007.
[26] F. Qu, J. Yang, and H. Zhang, Shape reconstruction in inverse scattering by an inhomogeneous cavity with internal measurements, *SIAM J. Imaging Sci.*, **12** (2019), 788–808.
[27] J. Xiang and G. Yan, The factorization method for inhomogeneous medium with an impenetrable obstacle, *Comp. Appl. Math.*, **40**, (2021), 270.
[28] J. Yang, B. Zhang, and H. Zhang, The factorization method for reconstructing a penetrable obstacle with unknown buried objects, *SIAM J. Appl. Math.*, **73** (2013), 617–635.
[29] J. Yang, B. Zhang, and H. Zhang, Near-field imaging of periodic interfaces in multilayered media, *Inverse Problems*, **32** (2016), 035010.
[30] J. Yang, B. Zhang, and H. Zhang, Uniqueness in inverse acoustic and electromagnetic scattering by penetrable obstacles, *J. Differ. Equ.*, **12** (2018), 6352–6383.
[31] H. Zhang and B. Zhang, A Newton method for a simultaneous reconstruction of an interface and a buried obstacle from far-field data, *Inverse Problems*, **29** (2017), 045009.
[32] F. Zeng, F. Cakoni, and J. Sun, An inverse electromagnetic scattering problem for a cavity, *Inverse Problems*, **27** (2011), 125002.
[33] F. Zeng, X. Liu, J. Sun, and L. Xu, The reciprocity gap method for a cavity in an inhomogeneous medium, *Inverse Probl. Imaging*, **10** (2016), 855–868.